



HAL
open science

Structural analysis of sulfate vein networks in Gale crater (Mars)

Barbara de Toffoli, Nicolas Mangold, Matteo Massironi, Alain Zanella, Riccardo Pozzobon, Stéphane Le Mouélic, Jonas L'Haridon, Gabriele Cremonese

► **To cite this version:**

Barbara de Toffoli, Nicolas Mangold, Matteo Massironi, Alain Zanella, Riccardo Pozzobon, et al.. Structural analysis of sulfate vein networks in Gale crater (Mars). *Journal of Structural Geology*, 2020, 137 (2), pp.104083. 10.1016/j.jsg.2020.104083 . hal-02933680

HAL Id: hal-02933680

<https://hal.science/hal-02933680>

Submitted on 8 Sep 2020

HAL is a multi-disciplinary open access archive for the deposit and dissemination of scientific research documents, whether they are published or not. The documents may come from teaching and research institutions in France or abroad, or from public or private research centers.

L'archive ouverte pluridisciplinaire **HAL**, est destinée au dépôt et à la diffusion de documents scientifiques de niveau recherche, publiés ou non, émanant des établissements d'enseignement et de recherche français ou étrangers, des laboratoires publics ou privés.

1 ***STRUCTURAL ANALYSIS OF SULFATE VEIN NETWORKS IN GALE***

2 ***CRATER (MARS)***

3
4 Barbara De Toffoli ^{a,b,d*}, Nicolas Mangold ^b, Matteo Massironi ^{a,d}, Alain Zanella ^c

5 Riccardo Pozzobon ^{a,d}, Stephane Le Mouélic ^b, Jonas L'Haridon ^b, Gabriele Cremonese ^d

6
7 ^a Department of Geosciences, University of Padova, Via Gradenigo 6, Padova 35131, Italy

8 ^b Laboratoire de Planetologie et Geodynamique, Universite de Nantes, CNRS UMR 6112, Nantes, France

9 ^c Department of Geology, Université du Maine, Le Mans, France

10 ^d INAF, Osservatorio Astronomico di Padova, Vicolo dell'Osservatorio 3, Padova I-35122, Italy

11 * Corresponding author: tel. +39 3772678273, email: barbara.detoffoli@unipd.it & barbara.detoffoli@gmail.com

12 **Abstract**

13 The Curiosity rover's campaign in the Gale crater on Mars provides a large set of close-up images
14 of sedimentary formations outcrops displaying a variety of diagenetic features such as light-toned
15 veins, nodules and raised ridges. Through 2D and 3D analyses of Mastcam images we herein
16 reconstruct the vein network of a sample area and estimated the stress field. Assessment of the
17 spatial distribution of light-toned veins shows that the basin infillings, after burial and
18 consolidation, experienced a sub-vertical compression and lateral extension coupled with fluid
19 overpressure and cracking. Overall, rock failure and light-toned veins formations could have been
20 generated by an overload produced by a pulse of infilling material within the basin.

21
22 **Keywords:** Mars – veins – fluid circulation – Curiosity rover – hydrofracturing

23

24

25 1. Introduction

26 NASA's Mars Science Laboratory mission, Curiosity, has been surveying the Gale crater since
27 August 2012. It is equipped with a set of 17 cameras and 10 scientific instruments that allow rock
28 and soil sample observation and analysis. Thanks to the *in situ* observations of the rover it has been
29 possible to recognize fluid circulation features emplaced during diagenesis subsequent to burial
30 and consolidation of the sediments. Specifically cross-cutting light-toned veins (Grotzinger et al.,
31 2014, L'Haridon et al., 2018; Nachon et al., 2014, 2017), nodules (Stack et al., 2014) and raised
32 ridges (Siebach et al., 2014; L veill  et al., 2014; McLennan et al., 2014) were detected. According
33 to ChemCam's Laser Induced Breakdown Spectroscopy (LIBS) measurements, the light-toned
34 veins have a Ca-sulfate mineralogy (Nachon et al., 2014) mainly interpreted to be bassanite
35 ($\text{CaSO}_4 \times 0.5 \text{H}_2\text{O}$) at least on the surface exposed portions of the investigated outcrops (Rapin et
36 al., 2016). These veins are observed throughout most of the outcrops recorded on the Curiosity
37 traverse, especially in the fine-grained sandstones and mudstones, interpreted to be fluvial and
38 lacustrine in origin (Grotzinger et al., 2014, 2015). The genesis of the veins is suggested to be
39 ascribable to fluid flows that led to dissolution and re-precipitation of sulfate-rich materials
40 (L'Haridon et al., 2018; Vaniman et al., 2018; Rapin et al., 2016; Schwenzer et al., 2016, Caswell
41 and Milliken, 2017). Veins with mineral infilling are associated to two main stages of formation:
42 i) the generation of fractures, which is a consequence of stresses and/or fluid overpressure
43 produced by several factors such as fluid thermal expansion, the generation of fluid (i.e. diagenetic
44 fluid expulsion), or chemical compaction; ii) the mineral infilling, which implies mineral
45 dissolution, transport and precipitation that may occur to form single or multiple veins (e.g.
46 Bj rlykke, 1997; Philipp, 2008). Thus fluids, a material source (with suitable T and P conditions
47 for precipitation) and fractures providing space for precipitation are the key ingredients to produce
48 a network of mineral veins such as the ones observed at Gale crater.

49 The purpose of this study is to assess the structural behaviour recorded by a well-exposed
50 crack system in a case study area along the rover traverse, to reconstruct the fracturing
51 mechanisms, deduce the pattern of stress during fluid circulation and therefore provide some
52 insights on the origin of the regional deformation involved during the formation of these features.

53 **2. Geological Background**

54 Gale is a complex crater located on the border of highlands close to the Martian dichotomy
55 (5.37°S, 137.81°W) and filled by sedimentary deposits forming a central mound, Aeolis Mons
56 (informally known as Mount Sharp). Gale crater is around 150 km in diameter and displays ~5 km
57 of elevation difference between the floor and the central peak and rims (Young and Chan, 2017;
58 Stack et al., 2016; Grotzinger et al., 2014, 2015; Le Deit et al., 2013; Wray, 2012). The meteor
59 impact that formed Gale crater has been estimated to have occurred around the Noachian-
60 Hesperian boundary (e.g. Le Deit et al., 2013; Thomson et al., 2011; Irwin et al., 2005). In the Late
61 Noachian/Early Hesperian epoch a major climatic change led water to be increasingly unstable at
62 surface conditions that Gale crater experienced and recorded. In fact, Gale crater has experienced
63 an intricate evolution involving the past presence of surface water indicated by rim-crossing carved
64 channels and lacustrine deposits at the mound base (e.g. Le Deit et al., 2013, Palucis et al., 2014,
65 Grotzinger et al., 2014; Thomson et al., 2011; Milliken et al., 2010), this site is invaluable for the
66 paleoenvironment reconstruction and pivotal for the investigation of Martian habitability (e.g.
67 Rubin et al., 2017, Caswell and Milliken, 2017).

68 Three main sedimentary groups have been identified in-situ by Curiosity rover investigations:
69 the Bradbury group, the Mount Sharp group and the Siccar Point group (Fig.1; Grotzinger et al.,
70 2014, 2015; Treiman et al., 2016). The first two groups are representative of a fluvio-lacustrine
71 environment recorded by laminated and cross stratified mudstones, sandstones and pebble
72 conglomerates, recognized especially at Pahrump Hills which is part of the Murray formation of
73 Mount Sharp group (e.g. Le Deit et al., 2016; Treiman et al., 2016; Stack et al., 2015; Bristow et

74 al., 2015; Grotzinger et al., 2014, 2015). The third group is dominated by eolian sedimentary rocks
75 that were accumulated unconformably over the other two and cemented (Banham et al., 2018).

76 Light-toned veins have been observed pervasively inside the Bradbury and Mount Sharp
77 group at a varying frequency (Watkins et al., 2017, L'Haridon et al., 2018). Some veins cross the
78 unconformity with the overlying eolian sedimentary rocks from the Siccar Point group (e.g.
79 Frydenvang et al., 2017) showing that some of them formed well-after the cementation and erosion
80 of the sedimentary layers. A remarkable part of the collected evidence related to the light-toned
81 veins are based on the compositional information acquired with ChemCam (Maurice et al., 2012;
82 Wiens et al., 2012) and its synergy with other instrument suites onboard Curiosity (e.g. CheMin,
83 Chemical and Mineralogy, and MAHLI, Mars Hand Lens Imager). The light-toned veins have a
84 calcium and sulfur-rich chemistry consistent with a Ca-sulfate mineralogy (Nachon et al., 2014),
85 mainly interpreted to be bassanite from the analysis of the hydrogen emission line (Rapin et al.,
86 2016).

87 The sedimentary rocks of interest for our work are located in the Murray formation, which is
88 at the base of the Mount Sharp group. The Murray formation is composed of mudstones
89 predominantly, with local fine-grained sandstones (Stein et al., 2018). An enhanced chemical
90 alteration has been suggested from the presence of a large fraction of phyllosilicates (up to 25% in
91 volume) and high values of chemical indices of alteration (Bristow et al., 2018, Mangold et al.,
92 2019). The Murray mudstones have been affected by a widespread post-depositional history as
93 observed through features such as fracture fills, veins, ridges and nodules, all indicating a complex
94 diagenetic history, not limited to the light-toned veins focused in our study (Grotzinger et al., 2015,
95 Nachon et al., 2017, L'Haridon et al., 2018). Investigating possible source of fluids that interplayed
96 in fractures development would lead to a better understanding of the sulfate veins' origins (e.g.
97 Schwenzer et al., 2016; Grotzinger et al., 2014, 2015, L'Haridon et al., 2018, Gasda et al., 2018).
98 Sources of sulfates have been suggested to be localized on higher (Nachon et al., 2017), lower
99 (Grotzinger et al., 2014; McLennan et al., 2014; Nachon et al., 2017) or lateral (McLennan et al.,

100 2014) layers with the respect of the fractured ones, whose fluid content underwent mobilization
101 during a late diagenetic event (Nachon et al., 2017; Young and Chan, 2017 and references therein).
102 Because of the ubiquitous presence of veins, a recent study proposed a paleoenvironmental
103 evolution at the entire basin scale that could lead to deposition, accumulation, burial, dissolution
104 and reprecipitation of the sulfates that filled the light-toned veins of Gale (Schwenzer et al., 2016).
105 The light-toned veins of the Gale Crater seem to be similar to those observed in many sedimentary
106 basins on Earth. This is especially the case for bedding-parallel fibrous gypsum veins called 'beef'
107 veins (Buckland & De La Bèche, 1835) or 'BPV' for Bedding-parallel veins (e.g. Ukar et al., 2017).
108 Several recent worldwide reviews demonstrate that these mineralized veins are very widespread
109 on Earth, especially within impermeable and anisotropic materials such as mudstones (Cobbold et
110 al., 2013; Gale et al., 2014). These veins are interpreted to be the result of fluid-assisted fracturing
111 due to pore fluid overpressures and stresses (e.g. Cobbold & Rodrigues, 2007; Cobbold et al.,
112 2013)

113 We collected structural data based on the distribution of light-toned veins distinguishable in
114 the area that the Curiosity rover observed between sol (Martian days)1536 and 1545 (Fig.1a).
115 While many outcrops of the Murray formation were either flat or partly buried below sand, this
116 location was chosen because of the presence of clean blocks, less than 1 m high, where light-toned
117 veins are visible enabling a detailed structural analysis using image analysis and photogrammetry
118 helped by the large number of image available.

119

120 **3. 3D reconstruction and measurements**

121

122 To investigate the light-toned veins that have been detected in Gale crater we performed 2D
123 and 3D analyses of Mastcam and Navcam Curiosity images. Mastcam takes colour images of 1600
124 × 1200 pixels that can be stitched together to create panoramas of the landscape around the rover.

125 Mastcam consists of a two-camera system that can acquire true RGB colour images, using a Bayer
126 filter, approximating what human eyes would perceive on Mars (Bell et al., 2012). With respect of
127 the scientific purpose of Mastcam, the Navcam camera pairs were planned for operational use
128 including acquisition of images for the rover's navigation, robotic planning and documentation,
129 remote sensing science instrument pointing, but also general surface imaging (Maki et al., 2011).
130 We coupled 2D mosaics of Mastcam images and the production of a 3D Digital Outcrop Model
131 (DOM) (e.g. Caravaca et al., 2019) of the same region from both Mastcam and Navcam in order
132 to reconstruct the fracture distribution in the area of interest which covers $\sim 100 \text{ m}^2$ (Fig.2).
133 2D images were observed raw and stitched together, where overlapping acquisitions of
134 neighbouring areas were available, in order to exploit full resolution image data for the detection
135 of fractures' characterizing marks (e.g. junctions and lateral continuity) and local distributions in
136 relation to other fracture sets and sediment laminations. We performed 3D reconstruction of the
137 same investigated outcrops by means of the Agisoft software (Wagner et al., 2014) from multiple
138 images taken by Mastcam binocular stereo vision and Navcam systems. Agisoft PhotoScan
139 (recently renamed Metashape) is a 3D advanced modelling package based on image data
140 processing which can automatically build the models without setting initial values and control
141 points. It processes images taken at any position and angle as far adjacent photos share
142 corresponding points recognizable on the targets. The scale computed by the software was tested
143 by comparing it with known size objects such as rovers' wheels. Loading the images into Agisoft,
144 the software automatically searches for the corresponding points matching and aligning the photos
145 and finally generating a sparse point cloud. When the automatic alignment procedure failed, tie
146 points were manually implemented in the system to exploit the maximum number of images
147 available. On the point cloud, that is generally denser closer to the observation point and
148 favourably oriented surfaces, an irregular triangle net can be built, then the texture mapping is
149 carried out according to the produced triangle net. We carried out the further step of elaboration
150 by using the Cloud Compare environment, which is a 3D point cloud and triangular mesh

151 processing software that allows the user to interact with 3D entities rotating, translating, drawing
152 2D polylines, picking points and extracting correspondent 2D and 3D information. In this context
153 veins were marked by tracing polylines and further structural information (i.e. dip direction and
154 dip angle, intersections angles, kinematics estimates) was developed by plane fitting and
155 contextual data extraction through the Cloud Compare compass plugin.

157 **4. Results**

158
159 Both from 2D images and 3D reconstruction, the presence of different sets of non-randomly
160 distributed fractures was neatly recognizable. All the fractures appear to have a higher resistance
161 against erosion with respect of the host rock, in fact they tend to stick out from the knobs leading
162 to an easy identification all over the outcrops. The first general distinction is the overall presence
163 of one population of bedding-parallel light-toned veins and a second population of middle to high-
164 angle dipping light-toned veins (Fig.3).

165 Bedding-parallel veins do not show significant thickness variations (averagely <1 cm) both at
166 the single vein scale and among the general population, although lateral continuity is unclear and
167 visible edges appear rounded and jagged, thus a patched distribution seems to be overall the most
168 reasonable. Bedding-parallel veins show a well recognizable undulate, slightly wandering trend as
169 recognizable in the measurements which display an averagely 15° dipping angle variation range
170 and a broad variability among the recorded dip directions (Fig.4g) due to the variability of the
171 available data, i.e. the outcropping visible veins, randomly sampling the undulate trend. Despite a
172 consistently average horizontal sub-parallel behaviour at the scale of the study area, bedding-
173 parallel veins show in places a cross cutting relationship bending and stopping on the neighbouring
174 ones (Fig.3b).

175 Oblique veins appear less frequent than the sub-horizontal population. These veins display
176 clear “en-echelon” structures well recognizable by the distinctive arrays of sigmoidal shaped

177 cracks (Nicholson and Pollard, 1985) that propagate from the margin of a larger parent crack,
178 twisting out and bending as the result of mechanical interaction between tips of adjacent parallel
179 cracks (Pollard et al. 1982). Such geometries are used to infer the state of deformation (Ramsay &
180 Huber 1983) or the state of stress (Pollard et al. 1982, Rickard & Rixon 1983) in the surrounding
181 rock at the time of cracking and accordingly, in the specificity of this case study, the “en-echelon”
182 features display an extensional component. We measured two different sets of oblique cracks
183 based on dip/dip-direction trends: (i) one with an average value of dip direction: 290°N and dip:
184 67° (spanning between minimum and maximum values of: 264°-309° dip direction and 54°-77°
185 dip) and a (ii) second one showing a dip direction-dip average value of 155°N - 53° (spanning
186 between minimum and maximum values of: 126°-184° dip direction and 31°-71° dip). On a
187 vertical section (as the ones provided by the outcrops walls facing toward the Curiosity rover), the
188 two populations of oblique fractures are thus intersecting at an average angle of 60° according to
189 the measurements, as illustrated by single outcrops where fractures from both the oblique sets are
190 visible (Fig.3).

191 In the study area it was also possible to observe cross-cutting relationships between the
192 different sets above distinguished by orientation. No evidence of displacement was found and
193 neither recurrent truncation of one set on the other were observed to determine an occurrence
194 sequence (Fig.3c).

195

196 **5. Discussions**

197

198 On Mars, the combination of 2D and 3D products on the Gale crater floor with high-resolution
199 in situ data along the rover track allows to pursue a structural interpretation of the basin at the time
200 of the generation of the light-toned veins. The general trend of all the plain sets to crosscut the host
201 rock laminations leads in first place to exclude a depositional layering interpretation. The presence

202 of two cross-cutting sets of light-toned vein sets arranged $\sim 60^\circ$ apart and displaying en-echelon
203 structures highlighting shear sense that led to a lowering of the hanging wall suggest an, at least
204 partial, regime of extension. Accordingly, the maximum principal stress is suggested to bisect the
205 acute angle occurring between the sets that in the specificity of this case would mean that σ_1 lays
206 on a sub-vertical axis. The minimum σ_3 orientation accordingly lays on a sub-horizontal plane and
207 displays NW-SE direction (Fig.4).

208 The set of horizontal veins is well-matching disposition and morphology of failures induced
209 by fluid overpressure recorded on Earth that happened during the fluid resurgence cracking the
210 host rock along fresh planes or exploiting previously existing surfaces of weakness such as the
211 mudstone bedding and laminations.

212 An example of the formation process that produced the horizontal vein set is the paleo-
213 hydrofracturing model of gypsum veins in the lower Mercia Mudstone Group (Philipp, 2008). This
214 group outcrops on the Somerset Coast of SW England, Watchet Bay, and display analogue
215 characteristics to the rocks observed in the Gale crater (e.g. Young and Chan, 2017; Cobbold et
216 al., 2013). The lower part of the Mercia Mudstone Group consists of several tens of meters of
217 poorly bedded, red to reddish-brown unfossiliferous mudstones and siltstones (Whittaker and
218 Green, 1983; Leslie et al., 1993), whereas in the upper part the red mudstones are characterized by
219 laterally discontinuous evaporite-rich horizons, mainly composed of white nodular gypsum
220 (Philipp, 2008). In the Mercia Mudstone Group vein dips show variations from horizontal to
221 vertical and the strikes are in broad range of directions, no clear predominant attitude was detected.
222 Crosscutting relationships were investigated as well and indicated no prevalent age relationship
223 suggesting that the veins may all have formed at the same time (Philipp, 2008). The formation is
224 interpreted to have formed in a playa lake or desert plain conditions (Bennison & Wright, 1969;
225 Simms & Ruffell, 1990), where ephemeral pools were likely to be present and remobilization and
226 accumulation of gypsum primarily disseminated in the sediment could have happened (Leslie et
227 al., 1993). In Watchet Bay fluid transport took place mainly along faults and fractures since

228 mudstones have a very low original permeability and are commonly effective barriers to fluid
229 circulation (Philipp, 2008; Cartwright, 1997). The outcrops show discontinuous anastomosing
230 networks of gypsum veins confined to portions of the hosting mudstone. The phenomenon is not
231 pervasive to the whole mudstone group though, but it is confined to specific portions often overlain
232 by thick grey siltstone layers weakly calcareous (Philipp, 2008). It may in fact occur that veins
233 produced by hydrofracturing stop where mechanical contrast boundaries occur (e.g. Brenner and
234 Gudmundsson, 2004b; Gudmundsson et al., 2002; Cosgrove, 2001; Gudmundsson and Brenner,
235 2001). There is no need of active slipping faults to allow fluid circulation and hydrofracturing, that
236 are triggered when the pressure of the fluids sited within the veins exceed the lithostatic pressure
237 (Ramsey, 1980). When fluids are involved (e.g. geothermal fluids), buoyancy overpressure can
238 convey a significant contribution to the fracturing process. Depending on the stress field, fluids
239 can be transported along the veins (i) leading to hydrofracturing propagation of already existing
240 fracture plains and anisotropies (i.e. bedding plains and laminations) or (ii) generating
241 hydrofracturing into the host rock (Philipp, 2008 and references therein). Philipp (2008) suggests
242 an hydrofracturing model to explain the sulphate vein network systems that cut the Mercia
243 Mudstone Group based on low permeability of the mudstone that drove fluids, flowing from the
244 highest to the lowest hydraulic potential (Domenico & Schwartz, 1998), to enter the rocks along
245 faults and fractures and prevented them to penetrate intimately the host rock.

246 The fluid source for the Martian case study is not entirely clear; fluid flow can be triggered by
247 very diverse physical and chemical disequilibria that might generate fluid overpressure. Some
248 examples could be compaction due to burial, diagenetic fluid expulsion and buoyancy,
249 crystallization, porosity changes and thermal expansion (Neuzil, 1995; Bjørlykke, 1997; Osborne
250 & Swarbrick, 1997). On Mars, Gale experienced water-rich early stages (Late Noachian/Early
251 Hesperian) during which the crater could have been connected to both surficial and underground
252 water reservoirs (e.g., Villanueva et al. 2015; Andrews-Hanna et al., 2010), thus implying

253 potentially transient flooding and drying in sabkha or ephemeral lake environments leading to
254 mineral (e.g. salts) precipitation and accumulation in the basin (Rapin et al., 2019).

255 Nevertheless, these veins are not likely to have formed early in the basin history, but when
256 compaction, consolidation and diagenetic processes started affecting the region. In fact a
257 significant part of the vein population consists of well recognisable fractures cross-cutting rock
258 bedding, hence the mudstone must have had some shear strength at the time of formation to trigger
259 a brittle response thus excluding a young soft host rocks (Schwenzer et al., 2016; Philipp, 2008;
260 Bell, 2000). Thus, subsequent dissolution and mobilization by diagenetic fluids of initial deposits,
261 of unclear stratigraphic position yet, may have led to the formation of the sulphate veins observed
262 on the rover traverse (L'Haridon et al., 2018; Schwenzer et al., 2016; Nachon et al., 2017;
263 Grotzinger et al., 2014; McLennan et al., 2014).

264

265 **6. Conclusions**

266

267 Light-toned fracture networks have been observed repeatedly along Curiosity rover traverse
268 (e.g. Watkins et al., 2017) and their distribution reflects the stress field they have been exposed to
269 at the moment of fracturing. Within the window of ten sols (sol 1536 – sol 1545) herein analysed,
270 Curiosity acquired a large number of images from different angles of a field of bedrock knobs
271 cropping out from the sand where many sulphate veins were neatly visible. This asset allowed the
272 3D reconstruction of the area and, contextually, the 3D reconstruction of the plane set where
273 fractures lay. On Earth, similar arrangements can be observed at Watchet Bay where networks of
274 intersecting sulphate veins developed thanks to hydrofracturing regimes within reddish mudstone
275 levels.

276 In Gale, the fracturing process is therefore to be ascribed to two different complementary
277 contributions: (i) the 60° dipping fractures are to be considered the product of an extensional
278 regime where the principal stress lays on a vertical axis (Fig.3a); (ii) the set of bedding-parallel

279 fractures are the result of a hydrofracturing process where fluid overpressure was energetic enough
280 to open new fractures just in places, but mostly used pre-existing weakness surfaces constituted
281 by mudstone layering. Additionally, the formation of the bedding-parallel vein set might have been
282 synchronous to the formation of the other two sets since no truncation or displacement have been
283 observed around the available outcrops. This interpretation is well supported by the geological
284 context. Gale is a large crater that experienced water and sediment infilling, the vertical maximum
285 stress is reasonably to be ascribed to such progressive overload. The cracking drive of
286 hydrofracturing, can be triggered either by the emplacement of an overburden that perturbs fluid
287 pressure, or as response to an unloading event when pressurized fluids are already stored in the
288 subsurface. The origin of fluids at Gale is still debated and overpressure cracking itself does not
289 carry enough information to discriminate it. In the hypothesis of a coeval genesis of the oblique
290 and the bedding-parallel vein networks, a pulse of material overload within the crater could have
291 been responsible both for the extensional failure and the fluid escape from the already consolidated
292 deposits on the crater floor. In this context, due to the crater circular shape, maximum extension is
293 accordingly expected to develop along the radial directions. This is confirmed by σ_3 NE-SW
294 direction recorded in the study area, σ_3 thus locally appears to develop radially compared to the
295 closest crater rim. However, to better constrain the scenario, it would be necessary to collect data
296 from multiple sites along the rover traverse in order to check the behaviour of σ_3 at different
297 position with the respect of the crater rim.

298 Veins mapping and reconstruction allowed the production of a well constrained structural
299 context interpretation and cracking driving forces identification which are likely to have been
300 active in the whole crater area so producing a structural context for the entirety of the fracture and
301 vein networks that have been recorded along the rover traverse.

302

303 **Acknowledgments**

304 This paper is part of a project supported by the European Union's Horizon 2020 research and
305 innovation program under grant agreement N°776276 (PLANMAP) and has been supported by the
306 “Fondazione Ing. Aldo Gini” scholarship. Some of the authors were funded by the Centre National
307 d’Etudes Spatiales (CNES). The data reported in this paper are archived at the Planetary Data
308 System, accessible at <http://pds-geosciences.wustl.edu/missions/msl/index.htm>. We are indebted
309 to the Mars Science Laboratory Project engineering and science teams for their diligent efforts in
310 making the mission as effective as possible and for their participations in tactical and strategic
311 operations.

312

313

References

314

- 315 Andrews-Hanna, J.C., et al., 2010. Early Mars hydrology: Meridiani playa deposits and the sedimentary record of
316 Arabia Terra. *J. Geophys. Res. E Planets* 115, 1–22. <https://doi.org/10.1029/2009JE003485>
- 317 Banham, S. G. et al. (2018) Ancient Martian aeolian processes and palaeomorphology reconstructed from the
318 Stimson formation on the lower slope of aeolis Mons, Gale Crater, Mars, *Sedimentology*, 65, 993-1042.
- 319 Bell, F. G., 2000. *Engineering Properties of Soils and Rocks*. Oxford: Blackwell.
- 320 Bell, J. F., et al., 2012. Mastcam multispectral imaging on the Mars Science Laboratory rover: wavelength
321 coverage and imaging strategies at the gale crater field site, *Lunar Plan. Sci. Conference*, pp 2541
- 322 Bennison, G. M. and Wright, A. E. 1969. *The Geological History of the British Isles*. London: Edward Arnold Ltd,
323 406 pp.
- 324 Bjørlykke, K. 1997. Lithological control on fluid flow in sedimentary basins. In *Fluid Flow and Transport in Rocks*
325 (eds B. Jamtveit & B. W. D. Yardley), pp. 15– 34. London: Chapman and Hall.
- 326 Brenner, S. L. & Gudmundsson, A. 2004b. Arrest and aperture variation of hydrofractures in layered reservoirs. In
327 *The Initiation, Propagation and Arrest of Joints and Other Fractures* (eds J. W. Cosgrove & T. Engelder), pp.
328 117–28. Geological Society of London, Special Publication no. 231.
- 329 Bristow, T. F., et al., 2015. The origin and implications of clay minerals from Yellowknife Bay, Gale crater, Mars,
330 *Am. Mineral.*, 100, 824–836, doi:10.2138/am-2015-5077CCBYNCND.
- 331 Buckland and De la Beche, 1835. On the Geology of the Neighbourhood of Weymouth and the Adjacent Parts of
332 the Coast of Dorset *Transactions of the Geological Society*, London 2–4, pp. 1–46

333 Caravaca, G.; Le Mouélic, S.; Mangold, N.; L'Haridon, J.; Le Deit, L.; Massé, M., 2019. 3D Digital Reconstruction
334 of the Kimberley Outcrop (Gale Crater, Mars) from Photogrammetry Using Multi-Scale Imagery from Mars
335 Science Laboratory 50th Lunar and Planetary Science Conference

336 Cartwright, J. A. 1997. Polygonal extensional fault systems: a new class of structure formed during the early
337 compaction of shales. In *Fluid Flow and Transport in Rocks* (eds B. Jamtveit & B. W. D. Yardley), pp. 35–
338 56. London: Chapman & Hall.

339 Caswell, T.E., Milliken, R.E., 2017. Evidence for hydraulic fracturing at Gale crater, Mars: implications for burial
340 depth of the Yellowknife Bay formation. *Earth Planet. Sci. Lett.* 468, 72–84. doi:10.1016/j.epsl.2017.03.033.

341 Cobbold, P.R., Zanella, A., Rodrigues, N., Løseth, H., 2013. Bedding-parallel fibrous veins (beef and cone-in-
342 cone): worldwide occurrence and possible significance in terms of fluid overpressure, hydrocarbon
343 generation and mineralization, *Mar. Pet. Geol.*, 43, pp. 1-20, 10.1016/j.marpetgeo.2013.01.010

344 Cobbold, P.R., Rodrigues, N., 2007. Seepage forces, important factors in the formation of horizontal hydraulic
345 fractures and bedding-parallel fibrous veins (“beef” and “cone-in-cone”), *Geofluids*, 7, pp. 313-322,
346 10.1111/j.1468-8123.2007.00183.x

347 Cosgrove, J.W., 2001. Hydraulic fracturing during the formation and deformation of a basin: A factor in the
348 dewatering of low-permeability sediments. *Am. Assoc. Pet. Geol. Bull.* 85, 737–748.
349 <https://doi.org/10.1306/8626C997-173B-11D7-8645000102C1865D>

350 Domenico, P. A. & Schwartz, F. W. 1998. *Physical and Chemical Hydrogeology*, 2nd ed. New York: Wiley, 506

351 Frydenvang J. et al., 2017. Diagenetic silica enrichment and late-stage groundwater activity in Gale crater, Mars.
352 *Geophys. Res. Lett.*, 44, 4716-4724.

353 Gale, J.F.W., Laubach, S.E., Olson, J.E., Eichhubl, P., FallA., 2014. Natural fractures in shale: A review and new
354 observations, *AAPG Bulletin*, 98 (11): 2165–2216. doi: <https://doi.org/10.1306/08121413151>

355 Gasda, P. J., et al. (2017) In situ detection of boron by ChemCam on Mars, *Geophysical Research Letters*, 44,
356 8739-8748.

357 Grotzinger, J.P., et al., 2014. A habitable fluvio-lacustrine environment at Yellowknife Bay, Gale crater, Mars.
358 *Science* (80–) 343 (6169). 1242777–1242777 doi: 10.1126/ science.1242777.

359 Grotzinger, J.P., et al., 2015. Deposition, exhumation, and paleoclimate of an ancient lake deposit, Gale crater,
360 Mars. *Science* (80–) 350 (6257). aac7575-aac7575 doi: 10.1126/science.aac7575.

361 Gudmundsson, A. & Brenner, S. L. 2001. How hydrofractures become arrested. *Terra Nova* 13, 456–62.

362 Gudmundsson, A., et al., 2002. Propagation pathways and fluid transport of hydrofractures in jointed and layered
363 rocks in geothermal fields. *Journal of Volcanology and Geothermal Research* 116, 257–78.

364 Hurowitz, J.A., Grotzinger, J.P., Fischer, W.W., McLennan, S.M., Milliken, R.E., Stein, N., Vasavada, A.R.,
365 Blake, D.F., Dehouck, E., Eigenbrode, J.L., Fairén, A.G., Frydenvang, J., Gellert, R., Grant, J.A., Gupta, S.,
366 Herkenhoff, K.E., Ming, D.W., Rampe, E.B., Schmidt, M.E., Siebach, K.L., Stack-Morgan, K., Sumner,
367 D.Y., Wiens, R.C., 2017. Redox stratification of an ancient lake in Gale crater, Mars. *Science* (80-.). 356.
368 <https://doi.org/10.1126/science.aah6849>

369 Irwin, R. P., A. D. Howard, R. A. Craddock, and J. M. Moore (2005), An intense terminal epoch of widespread
370 fluvial activity on early Mars: 2. Increased runoff and paleolake development, *J. Geophys. Res.*, 110,
371 E12S15, doi:10.1029/2005JE002460.

372 L'Haridon, J., Mangold, N., Meslin, P.-Y., Johnson, J. R., Rapin, W., Forni, O., et al. (2018). Chemical variability
373 in mineralized veins observed by ChemCam on the lower slopes of Mount Sharp in Gale crater, Mars. *Icarus*,
374 311, 69–86. <https://doi.org/10.1016/j.icarus.2018.01.028>

375 Le Deit, L., E. Hauber, F. Fueten, M. Pondrelli, A. P. Rossi, and R. Jaumann (2013), Sequence of infilling events in
376 Gale Crater, Mars: Results from morphology, stratigraphy, and mineralogy, *J. Geophys. Res. Planets*, 118,
377 doi:10.1002/2012JE004322.

378 Le Deit, L., et al., 2016. The potassic sedimentary rocks in Gale crater, Mars, as seen by ChemCam on board
379 Curiosity. *J. Geophys. Res. Planets* 121 (5), 784–804. doi:10.1002/2015JE004987.

380 Leslie, A. B., et al., 1993. Geochemical and mineralogical variations in the upper Mercia Mudstone Group (Late
381 Triassic), southwest Britain: correlation of outcrop sequences with borehole geophysical logs. *Journal of the*
382 *Geological Society, London* 150, 67–75.

383 Lèveillé, R.J., et al., 2014. Chemistry of fracture-filling raised ridges in Yellowknife Bay, Gale crater: window into
384 past aqueous activity and habitability on Mars. *J. Geophys. Res. Planets* 119 (11), 2398–2415.
385 doi:10.1002/2014JE004620.

386 Maki, J. N., et al., 2011. The Mars Science Laboratory (Msl) Navigation Cameras (Navcams), *Lunar Plan. Sci.*
387 Conference, pp 2738

388 Mangold, N., Dehouck, E., Fedo, C., Forni, O., Achilles, C., Bristow, T., Downs, R.T., Frydenvang, J., Gasnault,
389 O., L'Haridon, J., Le Deit, L., Maurice, S., McLennan, S.M., Meslin, P.Y., Morrison, S., Newsom, H.E.,
390 Rampe, E., Rapin, W., Rivera-Hernandez, F., Salvatore, M., 2019. Chemical alteration of fine-grained
391 sedimentary rocks at Gale crater. *Icarus* 321, 619–631.

392 Maurice, S. and 69 co-authors, 2012. The ChemCam instrument suite on the Mars Science Laboratory (MSL)
393 rover: Science objectives and mast unit description. *Space Sci. Rev.*, 170 :95-166, doi 10.1007/s11214-012-
394 9912-2.

395 McLennan, S.M., et al., 2014. Elemental geochemistry of sedimentary rocks at Yel-
396 lowknife Bay, Gale crater, Mars. *Science* (80-) 343 (6169), 1244734. doi:10.1126/
397 science.1244734.
398 Milliken, R.E., et al., 2010. Paleoclimate of Mars as captured by the stratigraphic record in Gale crater. *Geophys.*
399 *Res. Lett.* 37 (4), 1–6. doi:10.1029/2009GL041870.
400 Nachon, M., et al., 2014. Calcium sulfate veins characterized by ChemCam/Curiosity at Gale crater, Mars. *J.*
401 *Geophys. Res. Planets* 119 (9), 1991–2016. doi:10.1002/
402 2013JE004588.
403 Nachon, M., et al., 2017. Chemistry of diagenetic features analyzed by ChemCam at Pahrump Hills, Gale crater,
404 Mars. *Icarus* 281, 121–136. doi:10.1016/j.icarus.2016.08. 026.
405 Neuzil, C. E. 1995. Abnormal pressures as hydrodynamic phenomena. *American Journal of Science* 295, 742–86.
406 Nicholson, R. & Pollard, D.D. 1985. Dilation and linkage of en-echelon cracks. *Journal of Structural Geology*, 7,
407 583–590.
408 Osborne, M. J. & Swarbrick, R. E. 1997. Mechanisms for generating overpressure in sedimentary basins: A
409 reevaluation. *American Association of Petroleum Geologists Bulletin* 81, 1023–41.
410 Palucis, M., W. Dietrich, A. Hayes, R. Williams, S. Gupta, N. Mangold, H. E. Newsom, C. Hardgrove, F. Calef, D.
411 Sumner, 2014, The origin and evolution of the Peace Vallis fan system that drains to the Curiosity landing
412 area, Gale Crater, Mars, *J. Geophys. Res. Planets*, 119, 705–728, doi:10.1002/2013JE004583
413 Phillip, S. L., 2008. Geometry and formation of gypsum veins in mudstones at Watchet, Somerset, SW England,
414 *Geol. Mag.*, 145(6), 831–844, doi:10.1017/S0016756808005451.
415 Pollard, D. D., Segall, P. & Delaney, P. T. 1982. Formation and interpretation of dilatant echelon cracks. *Bull.*
416 *geol. Soc. Am.* 93, 1291-1303.
417 Rapin, W., et al., 2016. Hydration state of calcium sulfates in Gale crater, Mars: iden-
418 tification of bassanite veins. *Earth Planet. Sci. Lett.* 452, 197–205. doi:10.1016/j. epsl.2016.07.045.
419 Ramsay, J. G. 1980. The crack-seal mechanism of rock deformation. *Nature* 284, 135–9
420 Ramsay, J. G. & Huber. M. I. 1983. *The Techniques of Modern Structural Geology, Volume 1, Basic Techniques--*
421 *Strain Analysis.* Academic Press, London.
422 Rickard, M. J. & Rixon, L. K. 1983. Stress configurations in conjugate quartz-vein arrays. *J. Struct. Geol.* 5,573-
423 578.
424 Rubin, D.M., et al., 2017. Fluidized-sediment pipes in Gale crater, Mars, and possible Earth analogs. *Geology* 45,
425 7–10. <https://doi.org/10.1130/G38339.1>
426 Schwenzer, S.P., et al., 2016. Fluids during diagenesis and sulfate vein formation in sediments at Gale crater, Mars.
427 *Meteorit. Planet. Sci.* 28. doi:10.1111/maps. 12668.

426 Siebach, K.L., Grotzinger, J.P., Kah, L.C., Stack, K.M., Malin, M., Léveillé, R., Sum-
427 ner, D.Y., 2014. Subaqueous
428 shrinkage cracks in the Sheepbed mudstone: im-
429 plications for early fluid diagenesis, Gale crater, Mars. *J.*
430 *Geophys. Res. Planets* 119 (7), 1597–1613. doi:10.1002/2014JE004623.

429 Simms, M. J. and Rufell, A. H. 1990. Climatic and biotic change in the late Triassic. *Journal of the Geological*
430 *Society, London* 147, 321–7

431 Stack, K.M., et al., 2014. Diagenetic origin of nodules in the Sheepbed member, Yellowknife Bay formation, Gale
432 crater, Mars. *J. Geophys. Res. Planets* 119 (7), 1637– 1664. doi:10.1002/2014JE004617.

433 Stack, K. M., et al., 2015. Sedimentology and stratigraphy of the Pahrump Hills outcrop, lower Mount Sharp, Gale
434 Crater, Mars, 46 calcium sulfate veins as observed by the ChemCam instrument, 46 *Planetary Science*
435 *Conference*, 2 pp.

436 Stack, K. M., et al. 2016. Comparing orbiter and rover image-based mapping of an ancient sedimentary
437 environment, Aeolis Palus, Gale crater, Mars, *Icarus*, doi:10.1016/j.icarus.2016.02.024.

438 Thomson, B.J., et al., 2011. Constraints on the origin and evolution of the layered mound in Gale crater, Mars
439 using Mars Reconnaissance Orbiter data. *Icarus* 214 (2), 413–432. doi:10.1016/j.icarus.2011.05.002

440 Treiman, A.H., et al., 2016. Mineralogy, provenance, and diagenesis of a potassic basaltic sandstone on Mars:
441 CheMin X-ray diffraction of the Windjana sam-
442 ple (Kimberley area, Gale crater). *J. Geophys. Res. Planets*
443 121 (1), 75–106. doi:10.1002/2015JE004932.

443 Ukar, E., Lopez, R.G., Laubach, S.E., Gale, J.F.W., Manceda, R., Marrett R., 2017. Microfractures in bed-parallel
444 veins (beef) as predictors of vertical macrofractures in shale: Vaca Muerta Formation, Agrio Fold-and-Thrust
445 Belt, Argentina, *Journal of South American Earth Sciences*, 79, pp. 152-169, 10.1016/j.jsames.2017.07.015

446 Vaniman, D.T., et al., 2018. Gypsum, bassanite, and anhydrite at Gale crater, Mars. *Am. Mineral.* 103, 1011–1020.
447 <https://doi.org/10.2138/am-2018-6346>

448 Villanueva G. L. et al., 2015. Strong water isotopic anomalies in the Martian atmosphere: Probing current and
449 ancient reservoirs. *Science* 348:218–221.

450 Wagner, R. V., Henriksen, M.R., Manheim, M.R., Robinson, M.S., 2014. Photoscan for Planetary and Analogues
451 Sites, in: 3rd Planetary Data Workshop. p. 7023. <https://doi.org/10.1016/j.icarus.2014.04.002>

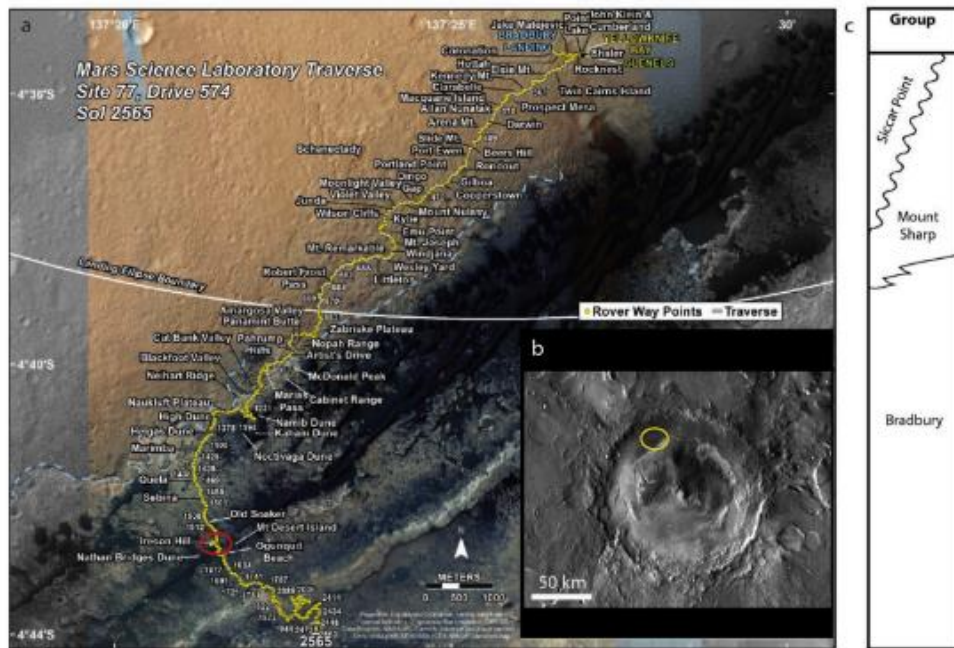
452 Watkins, J. A., et al., 2017. Fracture formation by compaction-related burial in Gale crater, Mars: implications for
453 the origin of Aeolis Mons, *Lunar Plan. Sci. Conference*, pp 3019

454 Whittaker, A. and Green, G. W. 1983. Geology of the country around Weston-super-Mare, memoir for 1:50,000
455 geological sheet 279. New series, with parts of sheet 263 and 295. Geological Survey of Great Britain,
456 Institute of Geological Sciences. London: Her Majesty's Stationery Office, 147 pp.

457 Wiens, R. C. and 80 co-authors, 2012. The ChemCam instrument suite on the Mars Science Laboratory (MSL)
458 rover: body unit and combined systems, *Space Sci. Rev.*, 170 :167-227, doi 10.1007/s11214-012-9902-4.
459 Wray, J. J., 2012. Gale crater: The Mars Science Laboratory/Curiosity Rover Landing Site, *Int. J. Astrobiol.*,
460 doi:10.1017/S1473550412000328.
461 Young, B.W., Chan, M.A., 2017. Gypsum veins in Triassic Moenkopi mudrocks of southern Utah: Analogs to
462 calcium sulfate veins on Mars. *J. Geophys. Res.* 150–171. <https://doi.org/10.1002/2016JE005118>
463

464

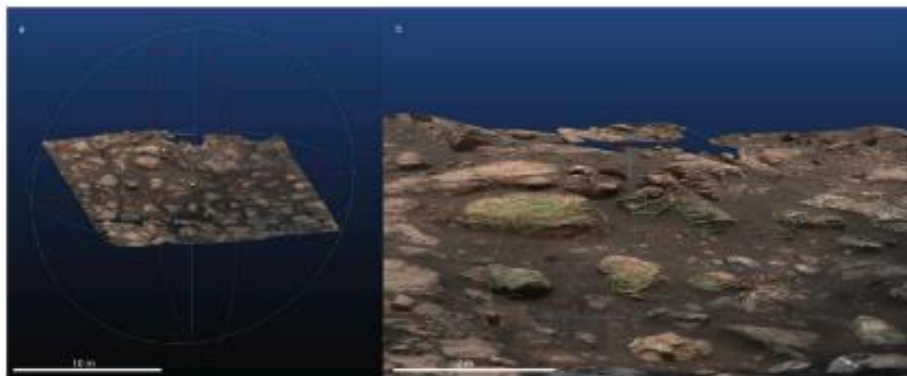
465 Figure 1. In panel (a) the yellow line with stops displays the Curiosity rover traverse; in the red
466 circle the study area is highlighted; the blue dashed line represents the contact between the
467 Bradbury group (NW) and the Mount Sharp group (SE). (b) Gale crater surveyed region. (c)
468 Stratigraphic column of Gale crater sedimentary rocks (modified after Hurowitz et al., 2017).



469

470

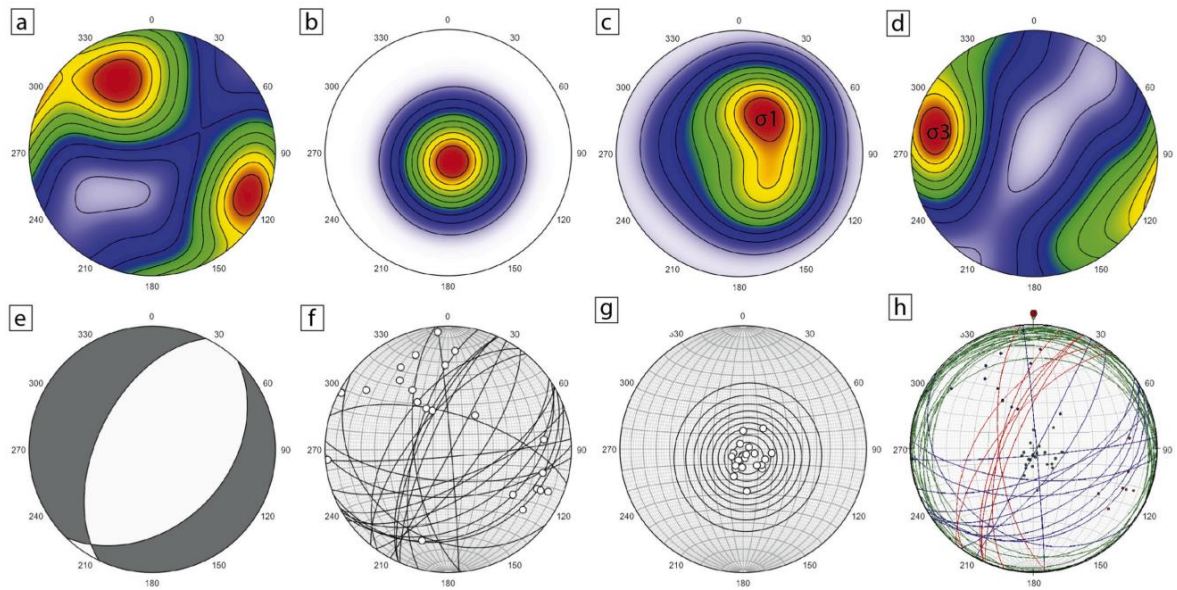
471 Figure 2. (a) 3D Digital Outcrop Model (DOM) of the region of interest within the area that
472 Curiosity rover observed between sol 1536 and 1545. (b) Computation output and histogram of
473 the point cloud volume density (green portions display maximum density values). (c)
474 Magnification of a portion of the study area. Plains are displayed on the texture and the dense point
475 cloud.



476

477

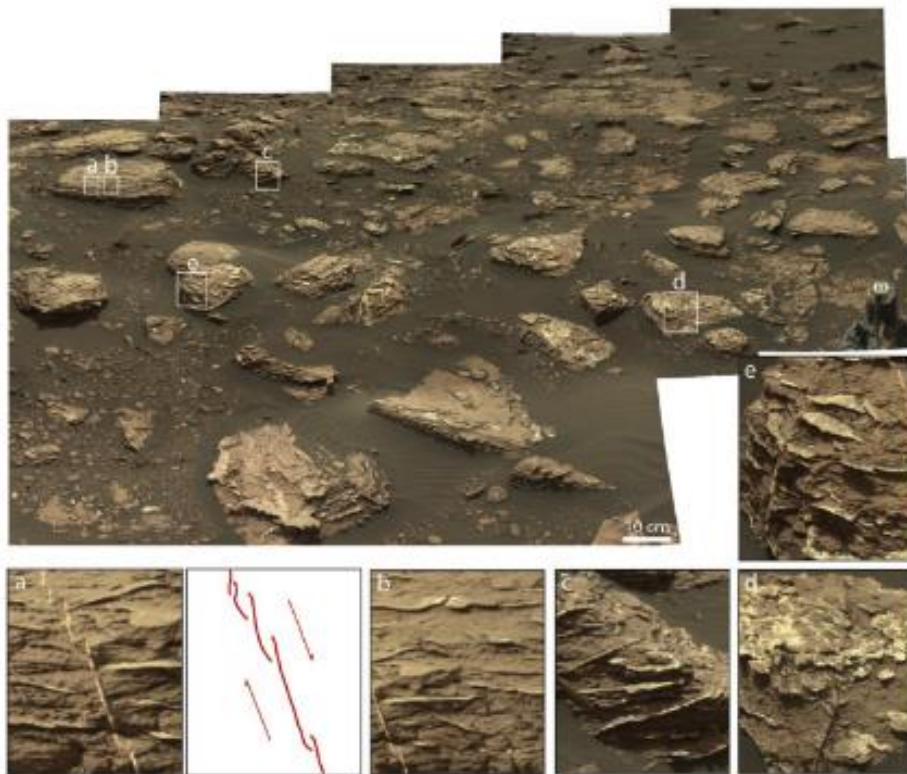
478 Figure 3. Stitched landscape of the main outcrop within the area of interest. The three different
479 identified sets are highlighted below. (a) oblique set of veins where “en-echelon” structures have
480 been recorded and preserved; (b) horizontal set, veins following the crosscutting lamination trend
481 are highlighted; (c) conjugate oblique vein set where the crosscutting relationship between sets is
482 well visible.



483

484

485 Figure 4. The stereo plots show: the orientation of the oblique (a,f) and bedding-parallel (b,g)
486 fracture planes detected on the study area on Mars; the maximum and minimum stress orientations
487 (c,d) and the kinematics extracted from the oblique vein set's data (e). Dataset extracted from the
488 3D DOM: 46 planes.



490